Nonlinear resonance and chaos in the relativistic phase space for driven nonlinear systems

Jung-Hoon Kim and Hai-Woong Lee
Department of Physics, Korea Advanced Institute of Science and Technology, Taejon 305-701, Korea
(Received 20 January 1995; revised manuscript received 21 March 1995)

We investigate the relativistic dynamics of a time-driven nonlinear system by analyzing the resonance structure in the relativistic phase space. It is shown that, when relativistic effects become appreciable, resonances that exist in the nonrelativistic description may be shifted or suppressed and resonances that are absent in the nonrelativistic description may be induced to appear. When these relativity-induced resonances overlap, the system exhibits chaotic relativistic motion. Numerical data that demonstrate such relativistic effects are presented with model systems of the driven Duffing oscillator and the driven Morse oscillator.

PACS number(s): 05.45.+b

I. INTRODUCTION

The classical chaotic dynamics of a time-driven nonlinear system can conveniently be described using the concept of resonance. It is well known, in particular, that the overlap between neighboring resonance zones induced in the system by the driving force signals the onset of classical chaos [1,2]. For determination of the critical force amplitude at which chaotic motion begins to occur, it therefore is important to know the structure of resonances, their locations and widths in particular. Much progress has been made in the past on ways to accurately determine the condition for the onset of chaos.

Up to now, much of the discussion of the resonance overlap and chaos has largely been limited to nonrelativistic systems. It has been known, however, that chaos can also be exhibited by systems undergoing relativistic motion [3–9] such as electrons in the free electron laser and the driven relativistic electron plasma wave, and significantly alter the operation of the systems. Perhaps the simplest system that can exhibit chaos at relativistic energies is the driven harmonic oscillator. As we have recently shown [3], when relativistic effects become appreciable, resonances are formed and chaos can be exhibited by the driven harmonic oscillator, although it is always associated with regular motion in the nonrelativistic regime.

In this paper we investigate the resonance structure of a driven nonlinear system in the relativistic phase space. We show, in particular, that when relativistic effects are fully considered, new resonances that are absent in the nonrelativistic description may appear in the high energy region. Just as in the nonrelativistic case, the overlap between these relativity-induced resonances can serve as a criterion for the onset of relativistic chaos.

II. RESONANCE ANALYSIS

Let us consider a one-dimensional system driven by a sinusoidal force of amplitude F_0 and frequency ω. The Hamiltonian for the system can be written as

$$H = \sqrt{p^2c^2 + m^2c^4} + V(q) + qF_0 \cos \omega t. \tag{1}$$

In the nonrelativistic limit ($mc^2 \gg pc$), the kinetic energy term becomes $mc^2 + \frac{p^2}{2m}$, yielding the standard nonrelativistic Hamiltonian. We consider the case where the type of motion shown by the system is oscillatory. For a given energy E, the system in the limit $F_0 \to 0$ may then be considered to oscillate between $q = a$ and $q = b$ ($b > a$), where a and b are the two roots for q of the equation

$$E - mc^2 = V(q). \tag{2}$$

The period-n resonance occurs at energy E at which the frequency ω of the driving force equals n times the frequency Ω of the oscillatory motion. Here we assume that the frequency of the oscillatory motion in the presence of the driving force is given approximately by that in the limit $F_0 \to 0$, which is valid as long as F_0 is not too great. The condition for the period-n resonance can then be expressed as

$$n = \frac{\omega}{\Omega(E)} = \omega \frac{\partial I(E)}{\partial E}, \tag{3}$$

where $I = I(E)$ is the action variable for the system in the limit $F_0 \to 0$, i.e.,

$$I = \frac{1}{2\pi} \oint p\, dq = \frac{1}{\pi c} \int_a^b \sqrt{[E - V(q)]^2 - m^2c^4}\, dq. \tag{4}$$

The action variable depends on energy E both because the integrand is a function of E and because the limits of integration, a and b, depend on E. Substitution of Eq. (4) into Eq. (3) yields

$$n = \frac{\omega}{\pi c} \int_a^b \frac{E - V(q)}{\sqrt{[E - V(q)]^2 - m^2c^4}}\, dq. \tag{5}$$

When energy E is sufficiently low that relativistic effects are negligible [$E - V(q) \cong mc^2$], Eq. (5) becomes

$$n \cong \frac{\omega\sqrt{2m}}{2\pi} \int_a^b \frac{dq}{\sqrt{E - mc^2 - V(q)}}, \tag{6}$$

yielding the standard resonance condition in the nonrelativistic regime. It is worth noting that, if the potential $V(q)$ varies with q more strongly than a harmonic potential, i.e., if the oscillator is "hard," the frequency $\Omega = 1/\frac{\partial I(E)}{\partial E}$ is an increasing function of energy E and thus a higher period resonance is formed at a lower energy. In the opposite case where the potential varies more slowly than a harmonic potential, i.e., when the oscillator is "soft," a higher period resonance appears at a higher energy.

In the ultrarelativistic limit where $E - V(q) \cong pc \gg mc^2$, Eq. (5) becomes

$$n \cong \frac{\omega(b-a)}{\pi c} = \omega \Big/ \left(\frac{\pi c}{b-a}\right). \tag{7}$$

We note that the quantity in the bracket on the right-hand side of Eq. (7) is just the frequency of the oscillatory motion when the speed of the oscillator is c. In normal situations the amplitude $(b-a)$ of oscillation is an increasing function of energy. Thus, according to Eq. (7), a higher period resonance is formed at a higher energy, regardless of whether the potential varies more rapidly or slowly than a harmonic potential.

It is interesting to note that the sequence of resonances in the relativistic region that appear in energy space is opposite to that in the nonrelativistic region, if the potential varies more rapidly than a harmonic potential, e.g., if $V(q) \propto |q|^3$ or q^4. In such a case, as one moves along the energy axis from low toward high energy, one encounters a series of resonances in the order of decreasing period in the nonrelativistic region, followed by another series of resonances in the order of increasing period in the relativistic region. The latter series of resonances arises solely from relativistic considerations and thus is referred to as relativity-induced resonances. The former exists in both nonrelativistic and relativistic descriptions and is simply referred to as nonrelativistic resonances.

If the potential varies more slowly than a harmonic potential, the orders in which nonrelativistic and relativistic resonances appear are the same. This means that relativistic considerations should have an effect of simply shifting the location of each nonrelativistic resonance. There will be no newly generated or suppressed resonances, and relativistic effects show up in a less dramatic way for a soft oscillator.

III. EXAMPLES

As examples to demonstrate the relativistic effects described in the previous section, we consider the Duffing double-well oscillator and the Morse oscillator. The Duffing oscillator at high energies behaves as a "hard" oscillator, whereas the Morse oscillator is an example of a "soft" oscillator. One thus expects to see relativity-induced and suppressed resonances for the case of the Duffing oscillator, while only a shift in the positions of resonances is expected to occur in the Morse oscillator.

A. Driven Duffing oscillator

Our first example is the Duffing double-well oscillator driven by a sinusoidal force. The potential is taken to be

$$V(q) = -\tfrac{1}{4}q^2 + \tfrac{1}{8}q^4. \tag{8}$$

This potential has a minimum value of $-\frac{1}{8}$ at $q = \pm 1$. For convenience of our discussion of relativistic effects, we fix the oscillator mass and the driving frequency to be $m = 1$ and $\omega = \frac{\pi}{2}$, and vary the value of c. The nonrelativistic limit corresponds to $c \to \infty$, and relativistic effects become stronger as one takes a smaller value of c.

The phase-space map of the oscillator can be constructed by numerically following the motion governed by the relativistic Hamilton's equations

$$\frac{dq}{dt} = \frac{p}{\sqrt{m^2 + p^2/c^2}}, \tag{9}$$

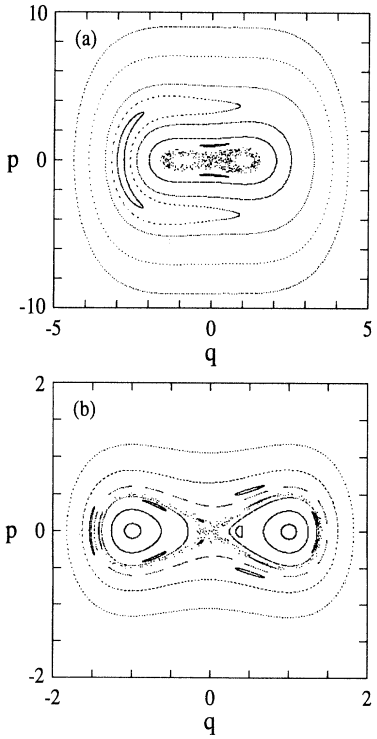

FIG. 1. Phase-space maps for the driven Duffing oscillator with the oscillator mass $m = 1$ and the driving frequency $\omega = \frac{\pi}{2}$ in a unit system in which the speed of light, $c \to \infty$. The amplitude of the driving force is 0.1 for (a) and 0.01 for (b).

TABLE I. The location (q,p) of one of the fixed points of each resonance present in Fig. 1, and the corresponding resonance energy $E - mc^2$ computed numerically from the (q,p) values and calculated theoretically based on the resonance analysis. L and R in the first column refer to resonances corresponding to motion confined in the left and right wells, respectively. The speed of light, c, is taken to be $c \to \infty$.

			$E - mc^2$	
n	q	p	Numerical	Theoretical
L2	-0.69	0.35	-0.029	-0.031
R2	0.37	0	-0.032	-0.031
5	-1.42	0	0.004	0.007
3	-1.53	0	0.100	0.101
1	-2.91	0	6.82	6.62

$$\frac{dp}{dt} = \tfrac{1}{2}q - \tfrac{1}{2}q^3 - F_0 \cos \omega t. \tag{10}$$

We show in Figs. 1–4 phase-space maps for the cases $c = \infty$, 5.5, 0.5, and 0.2, respectively. Plot (a) in each figure was drawn at the force amplitude $F_0 = 0.1$ and gives a broad view of high-energy resonances, while plot (b) drawn at $F_0 = 0.01$ shows a more detailed view of low-energy resonances not apparent in plot (a). The location of the resonances found in each figure is tabulated in Tables I–IV. The q and p values represent the location of one of the fixed points of each resonance, and the column under "numerical" gives corresponding values of resonance energy $E - mc^2$ computed from the q and p values.

In the nonrelativistic plot ($c \to \infty$) of Fig. 1(a) the period-1 resonance centered at $q \cong -2.9$, $p = 0$ is clearly seen, while the period-3 resonance formed at a lower energy is only barely seen as it lies in the chaotic region. Higher-period resonances lying at even lower energies seem to have already been destroyed at $F_0 = 0.1$. Figure 1(b) drawn at a lower value 0.01 of F_0 shows the period-3 resonance clearly separated from the chaotic region and the period-5 resonance that was absent in Fig. 1(a). Apparently at the low value (0.01) of F_0 at which Fig. 1(b) was drawn, the period-5 resonance still survives. Also shown is a pair of period-2 resonances at $E - mc^2 \cong -0.03$, which arise from the motion confined in one of the two wells. There is no period-1 resonance in the region $E - mc^2 < 0$, because the frequency Ω of the motion remains less than 1 (it approaches 1 only in the limit $E \to V_{\min} = -\frac{1}{8}$) and thus can never be equal to $\omega = \frac{\pi}{2}$.

TABLE II. Same as Table I except $c = 5.5$.

			$E - mc^2$	
n	q	p	Numerical	Theoretical
L2	-0.69	0.35	-0.030	-0.032
R2	0.37	0	-0.032	-0.032
5	-1.42	0	0.004	0.007
3	-1.53	0	0.100	0.103
1	-3.50	0	15.64	15.13
1	4.67	0	54.24	53.91

At $c = 5.5$, we see no significant change in the resonance structure from the one in the nonrelativistic limit,

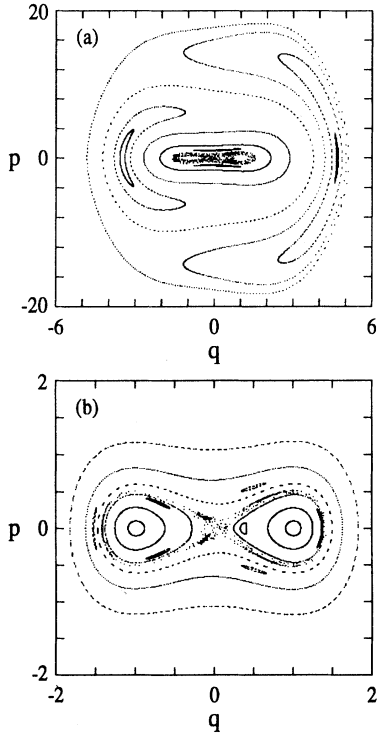

FIG. 2. Same as Fig. 1 except $c = 5.5$.

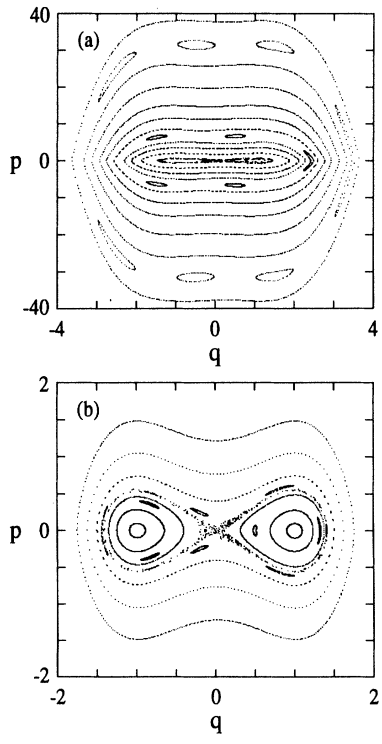

FIG. 3. Same as Fig. 1 except $c = 0.5$.

TABLE III. Same as Table I except $c = 0.5$.

			$E - mc^2$	
n	q	p	Numerical	Theoretical
L2	-0.82	0.36	-0.052	-0.054
R2	0.50	0	-0.055	-0.054
L3	-0.12	0	-0.004	-0.004
R3	1.41	0	-0.003	-0.004
5	-1.44	0	0.018	0.019
5	2.45	0	3.028	3.022
7	3.49	0	15.44	15.43

TABLE IV. Same as Table I except $c = 0.2$.

			$E - mc^2$	
n	q	p	Numerical	Theoretical
L2	-0.95	0.26	-0.099	-0.099
R2	1.21	0	-0.098	-0.099
L3	-0.42	0	-0.040	-0.040
R3	1.35	0	-0.040	-0.040
9	-1.42	0	0.003	0.003
9	1.78	0	0.455	0.453
11	2.19	0	1.676	1.675

except that, in addition to the period-1 resonance centered at $q \cong -3.5$, $p = 0$, corresponding to $E - mc^2 \cong 15.6$, there is a new period-1 resonance at $q \cong 4.7$, $p = 0$, corresponding to a higher energy of $E - mc^2 \cong 54.2$. This resonance is clearly absent in the nonrelativistic plot of Fig. 1 and thus represents a resonance induced by relativity.

At $c = 0.5$, we see from Fig. 3(a) that two relativity-induced resonances of period 5 and period 7 are formed. That these are relativity-induced resonances is clear because the period-7 resonance lies at a higher energy than the period-5 resonance, in opposition to the nonrelativistic situation of Fig. 1 where a higher-period resonance is formed at a lower energy. It should be noted that, at $c = 0.5$, the energy at which the period-1 or period-3 resonance would be formed is already relativistic. The period-1 and period-3 nonrelativistic resonances are thus suppressed by relativity, while at the same time a new series of resonances starting with that of period 5 are induced by relativity. The period-5 nonrelativistic resonance can be seen in Fig. 3(b) along with pairs of period-2 and period-3 resonances in the region $E - mc^2 < 0$.

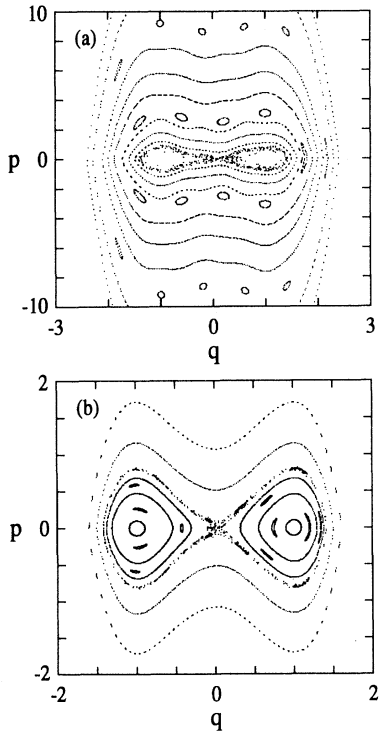

FIG. 4. Same as Fig. 1 except $c = 0.2$.

At $c = 0.2$ we see from Fig. 4(a) that two relativity-induced resonances of period 9 and period 11 are formed. At the same time the period-9 nonrelativistic resonance can barely be seen in Fig. 4(b) as it lies in the chaotic region. Apparently at $c = 0.2$ the nonrelativistic resonances of period lower than 9 have disappeared and are replaced by a series of relativity-induced resonances starting with that of period 9. Also seen in Fig. 4(b) are pairs of period-2 and period-3 resonances in the region $E - mc^2 < 0$.

The complex resonance structure shown in Figs. 1–4 and tabulated in Tables I– IV can best be explained using the analysis described in Sec. II. The resonance condition for the case of the Duffing oscillator can be written as (considering the case where $E - mc^2 > 0$)

$$n = \omega \frac{\partial I(E)}{\partial E} = \frac{2\omega}{\pi c} \int_0^b \frac{E + \frac{q^2}{4} - \frac{q^4}{8}}{\sqrt{(E + \frac{q^2}{4} - \frac{q^4}{8})^2 - m^2c^4}} dq, \tag{11}$$

where the amplitude $b = b(E)$ of the oscillatory motion is by Eq. (2)

$$E - mc^2 = -\tfrac{1}{4}b^2 + \tfrac{1}{8}b^4. \tag{12}$$

In Figs. 5–8 we plot $\omega \frac{\partial I(E)}{\partial E}$ computed by numerically integrating Eq. (11) as a function of $(E - mc^2)$ for the cases $c = \infty$, 5.5, 0.5, and 0.2, respectively. Plot (a) in each figure is drawn for the energy range $0 \leq E - mc^2 \leq 100$ (for Figs. 5 and 6) or $0 \leq E - mc^2 \leq 10$ (for Figs. 7 and 8), while plot (b) shows a more detailed view of the low energy region including the negative energy region, i.e., $-\frac{1}{8} \leq E - mc^2 \leq 0.2$. The energy at which the period-n resonance is formed can be found by reading the value of E corresponding to the crossing point of the horizontal line of constant n with the curve in the figures.

In the nonrelativistic limit ($c = \infty$), we see from Fig. 5(a) that, for $E - mc^2 > 0$, $\omega \frac{\partial I(E)}{\partial E}$ is a monotonically decreasing function of energy, approaching 0 as $E - mc^2 \to \infty$. Thus, as we move from $E - mc^2 = 0$ to $E - mc^2 \to \infty$, we encounter resonances of decreasing period all the way down to $n = 1$. Figure 5(b) indicates that this sequence of resonances is reversed for $E - mc^2 < 0$. Thus, a higher-period resonance is formed at a higher en-

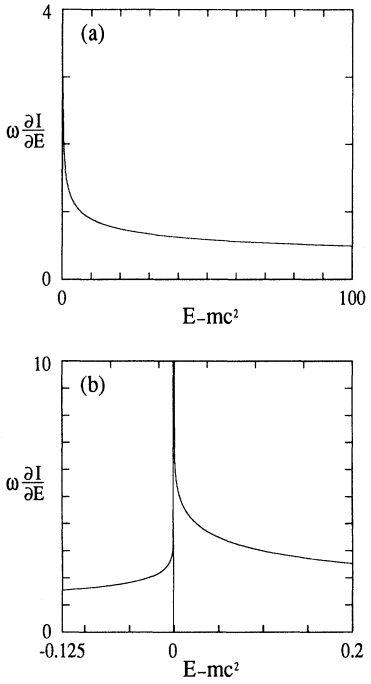

FIG. 5. $\omega\frac{\partial I(E)}{\partial E}$ vs $(E-mc^2)$ for the driven Duffing oscillator with the oscillator mass $m=1$ and the driving frequency $\omega=\frac{\pi}{2}$ in a unit system in which the speed of light, $c\to\infty$. The energy range plotted is $0\le E-mc^2\le 100$ for (a) and $-\frac{1}{8}\le E-mc^2\le 0.2$ for (b).

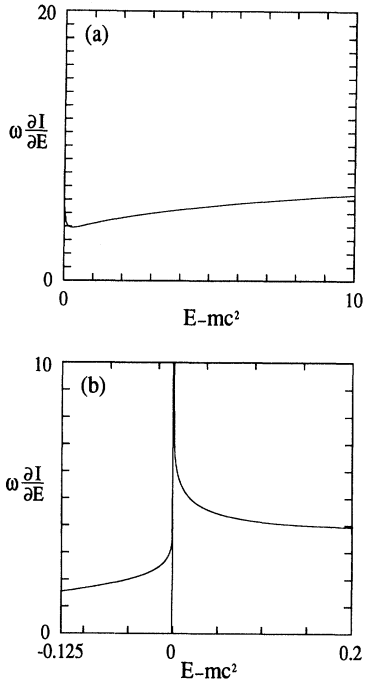

FIG. 7. Same as Fig. 5 except $c=0.5$, and the energy range plotted is $0\le E-mc^2\le 10$ for (a).

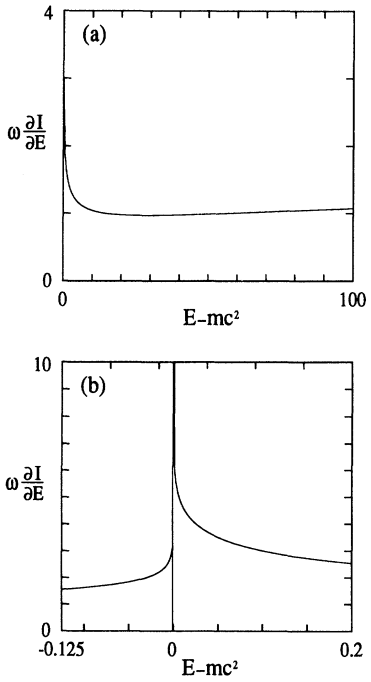

FIG. 6. Same as Fig. 5 except $c=5.5$.

ergy for $E-mc^2<0$. We should also note that $\omega\frac{\partial I(E)}{\partial E}$ approaches $\frac{\pi}{2}$ as $E-mc^2\to-\frac{1}{8}$, the minimum value of the potential.

Comparing Figs. 6(a), 7(a), and 8(a) with Fig. 5(a), the most significant change that occurs in the plot when relativistic effects are taken into account is that the func-

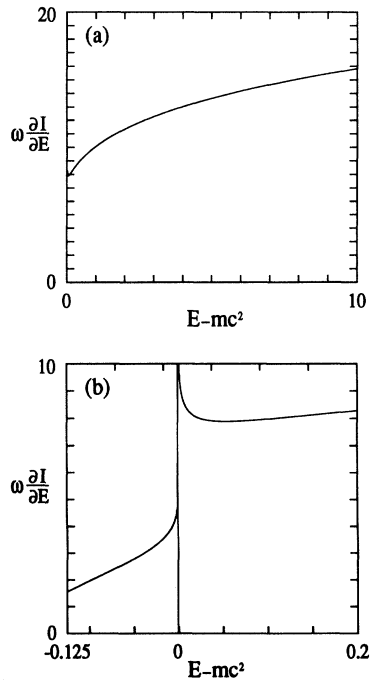

FIG. 8. Same as Fig. 7 except $c=0.2$.

tion $\omega\frac{\partial I(E)}{\partial E}$ does not monotonically decrease with energy. Instead, it is seen to reverse its direction at some point and begin increasing with energy apparently to ∞ as $E - mc^2 \to \infty$. This means that, in addition to the resonances that already exist in the nonrelativistic description, there appears a new series of high-energy resonances when relativistic effects are properly taken into account. Comparison of Figs. 6(b), 7(b), and 8(b) with Fig. 5(b) indicates, however, that relativistic effects do not cause any such qualitative change in the plot for the region $E - mc^2 < 0$. Here, only the locations of the resonances are shifted when relativistic effects are considered.

Although not apparent in Fig. 6(a), the equation $n = \omega\frac{\partial I(E)}{\partial E}$ for $c = 5.5$ has a pair of roots for all values of positive integers including $n = 1$. Thus, at $c = 5.5$, there exist two complete series of resonances, nonrelativistic and relativity induced, provided that the amplitude of the driving force is sufficiently small that the resonances are not destroyed. The function $\omega\frac{\partial I(E)}{\partial E}$, however, increases with energy very slowly in the region where low-period relativity-induced resonances are formed. As a result, the period-3 relativity-induced resonance appears at a relatively high energy which is outside the range of Fig. 2(a). This is why period-3 and higher-period relativity-induced resonances are not seen in Fig. 2(a).

Figures 7(a) and 8(a) indicate that, as relativistic effects become stronger, the curve of $\omega\frac{\partial I(E)}{\partial E}$ vs $(E - mc^2)$ reverses its direction sooner and the minimum value of the curve gets greater. As a result, the curve of Fig. 7(a) has no root for odd integers 3 and 1, and that of Fig. 8(a) has no root for odd integers smaller than 9. This explains why at $c = 0.5$ the period-1 and period-3 nonrelativistic resonances disappear and a new series of relativity-induced resonances starting with the period-5 resonance appear. At $c = 0.2$ relativistic effects are even stronger, and the four lowest-period nonrelativistic resonances are suppressed and the relativity-induced resonances start with one of period 9. Figures 7(a) and 8(a) show that one can simultaneously observe resonances suppressed by relativity and induced by relativity in the same system.

In Tables I–IV we list the theoretical values $E - mc^2$ of the resonance energy obtained by solving Eq. (11) based on the analysis presented in this section for all resonances observed in Figs. 1–4. The agreement with the numerical values is good in all cases.

B. Driven Morse oscillator

As a second example, we consider a one-dimensional Morse oscillator driven by a sinusoidal force. The potential is given by

$$V(q) = D[1 - e^{-\alpha(q-q_e)}]^2. \tag{13}$$

The initial energy of the oscillator is assumed to be sufficiently below D so that its motion is basically of oscillatory type. Hamilton's equations of motion now take the form

$$\frac{dq}{dt} = \frac{p}{\sqrt{m^2 + p^2/c^2}}, \tag{14}$$

$$\frac{dp}{dt} = -2D\alpha e^{-\alpha(q-q_e)}[1 - e^{-\alpha(q-q_e)}] - F_0\cos\omega t. \tag{15}$$

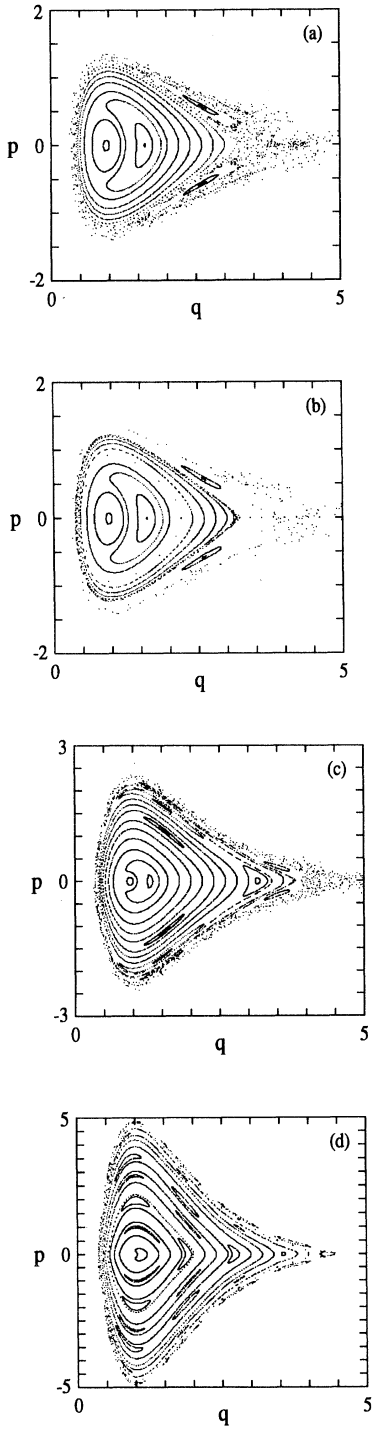

FIG. 9. Phase-space maps for the driven Morse oscillator with the oscillator mass $m = 1$, potential parameters $D = 1$, $\alpha = 1$, $q_e = 1$, and the driving frequency $\omega = 0.9 \times \sqrt{2}$ and the amplitude of the driving force $F_0 = 0.02$. The speed of light, c, is ∞ for (a), 5.5 for (b), 0.5 for (c), and 0.2 for (d).

TABLE V. The location (q,p) of one of the fixed points of each resonance present in Fig. 9, and the corresponding resonance energy $E - mc^2$ computed numerically from the (q,p) values and calculated theoretically based on the resonance analysis.

				$E - mc^2$	
c	n	q	p	Numerical	Theoretical
∞	1	1.612	0	0.2095	0.1900
	2	2.613	0.566	0.8013	0.7975
5.5	1	1.605	0	0.2060	0.1864
	2	2.593	0.574	0.7990	0.7950
0.5	1	1.296	0	0.0656	0.0557
	2	1.538	1.115	0.5341	0.5331
	3	3.157	0	0.7820	0.7795
0.2	1	1.133	0	0.0155	0.0117
	2	1.110	0.962	0.1674	0.1674
	3	1.913	0	0.3584	0.3572
	4	0.928	2.839	0.5348	0.5348

A theoretical analysis of nonlinear resonances and their overlap in the driven nonrelativistic Morse oscillator has been given earlier [10]. We are interested in any modifications that are necessary when the motion becomes relativistic.

Phase-space maps obtained by numerically integrating Eqs. (14) and (15) are shown in Fig. 9 for the cases $c = \infty$, 5.5, 0.5, and 0.2, with the parameters $m = 1$, $D = 1$, $\alpha = 1$, $q_e = 1$, $\omega = 0.9 \times \sqrt{2}$, and $F_0 = 0.02$. We note that at energy slightly above zero the natural frequency of the oscillator is $\sqrt{2D\alpha^2/m} = \sqrt{2}$. Since the frequency of the driving force is taken to be $\omega = 0.9\times\sqrt{2}$, resonances of all integer periods including $n = 1$ should be formed. The nonrelativistic plot of Fig. 9(a) shows the period-1 resonance centered at $q \cong 1.6$, $p = 0$, corresponding to $E - mc^2 \cong 0.21$, and the period-2 resonance centered at $q \cong 2.6$, $p \cong \pm 0.57$, corresponding to $E - mc^2 \cong 0.80$. Since the Morse potential is not symmetric, resonances of even periods appear along with those of odd periods. At $c = 5.5$ we see from Fig. 9(b) that no significant change has occurred from the nonrelativistic structure. Figure 9(c) indicates, however, that at $c = 0.5$ resonances are seen to be shifted toward lower energies, with the period-1 resonance formed at $E - mc^2 \cong 0.066$ and the period-2 resonance at $E - mc^2 \cong 0.53$. In addition, resonance of period 3 appears at $E - mc^2 \cong 0.78$. At $c = 0.2$ we see from Fig. 9(d) that resonances are shifted further toward lower energies and resonances of periods 1 – 5 can be clearly identified. In order to help identifying the resonances we tabulate in Table V locations of the resonances found in Fig. 9.

As in the case of the Duffing oscillator, the locations of the resonances can be estimated by using Eq. (5). For the present case of the Morse oscillator one of course needs to substitute Eq. (13) into Eq. (5). The right-hand side of Eq. (3), $\omega\frac{\partial I(E)}{\partial E}$, so computed is plotted as a function of energy E in Fig. 10 for the cases $c = \infty$, 5.5, 0.5, and 0.2. We note that the curve for $c = 5.5$ is indistinguishable from the curve for $c = \infty$ with the scale drawn here. It should be obvious, however, that, as relativistic effects become stronger, $\omega\frac{\partial I(E)}{\partial E}$ increases faster with respect to energy, and consequently resonances are formed at lower energies, consistent with the observation made from the phase-space maps. The theoretical values of the resonance energy estimated based on Fig. 10 are listed in Table V alongside the numerical values computed based on the phase-space maps. The agreement between the two sets is good in all cases.

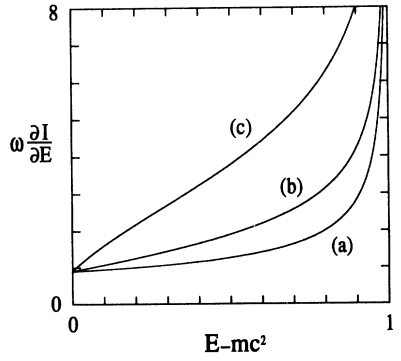

FIG. 10. $\omega\frac{\partial I(E)}{\partial E}$ vs $(E - mc^2)$ for the driven Morse oscillator with the oscillator mass $m = 1$, potential parameters $D = 1$, $\alpha = 1$, $q_e = 1$, and the driving frequency $\omega = 0.9\times\sqrt{2}$. The speed of light c is taken to be ∞ (or 5.5) for (a), 0.5 for (b), and 0.2 for (c).

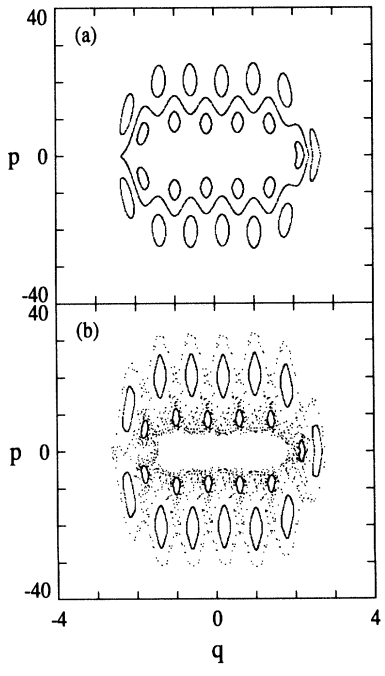

FIG. 11. Phase-space maps for the driven Duffing oscillator with the oscillator mass $m = 1$ and the driving frequency $\omega = \frac{\pi}{2}$ in a unit system in which the speed of light $c = 0.2$. The amplitude of the driving force is 3.75 for (a) and 7.5 for (b).

C. Resonance overlap and chaos

It should be noted that in general relativity-induced resonances are further apart from each other than the standard nonrelativistic resonances are from each other. All the relativity-induced resonances shown in Figs. 2–4 and Fig. 9 are thus well defined and free from overlap. Nevertheless, these resonances do overlap at a sufficiently high force amplitude and chaotic behavior can be observed in the relativistic phase space.

An illustration is provided in Figs. 11(a) and 11(b), where phase-space maps of our Duffing oscillator are shown for $c = 0.2$ at two different values of the force amplitude, $F_0 = 3.75$ and $F_0 = 7.5$, respectively. It is clear that at $F_0 = 7.5$ the two relativity-induced resonances, the period-11 and period-13 resonances, overlap and the system exhibits chaos in the relativistic phase space.

IV. SUMMARY

In summary we have shown that resonances that exist in the nonrelativistic description can be shifted or suppressed and new resonances that do not exist in the nonrelativistic description can be generated, when relativistic effects become appreciable. If the oscillator is softer than the harmonic oscillator, then only the shift of resonances can occur. If, however, the oscillator is harder than the harmonic oscillator, the generation and/or suppression of resonances can take place. The significance of the newly generated relativistic resonances lies in the fact that, when the driving force is sufficiently strong that the overlap between the relativity-induced resonances occur, chaotic relativistic motion is exhibited by the system. The work reported here can be useful, for example, in studies of the dynamics of driven relativistic electron plasma waves [7] which can be modeled by driven nonlinear oscillators.

ACKNOWLEDGMENTS

This research was supported in part by the Agency for Defense Development and by a KAIST Research Grant.

[1] B. V. Chirikov, Phys. Rep. **52**, 263 (1979).
[2] D. F. Escande and F. Doveil, J. Stat. Phys. **26**, 257 (1981).
[3] J. H. Kim and H. W. Lee, Phys. Rev. E **51**, 1579 (1995).
[4] C. Chen and R. C. Davidson, Phys. Rev. A **42**, 5041 (1990); Phys. Fluids B **2**, 171 (1990); Phys. Rev. Lett. **72**, 2195 (1994).
[5] A. A. Chernikov, T. Tél, G. Vattay, and G. M. Zaslavsky, Phys. Rev. A **40**, 4072 (1989); A. A. Chernikov and G. Schmidt, Chaos **3**, 525 (1993).
[6] M. Billardon, Phys. Rev. Lett. **65**, 713 (1990).
[7] W. P. Leemans, C. Joshi, W. B. Mori, C. E. Clayton, and T. W. Johnston, Phys. Rev. A **46**, 5112 (1992).
[8] A. Chao, D. Johnson, S. Peggs, J. Peterson, C. Saltmarsh, L. Schachinger, R. Meller, R. Siemann, R. Talman, P. Morton, D. Edwards, D. Finley, R. Gerig, N. Gelfand, M. Harrison, R. Johnson, N. Merminga, and M. Syphers, Phys. Rev. Lett. **61**, 2752 (1988).
[9] W. C. Schieve and L. P. Horwitz, Phys. Lett. A **156**, 140 (1991).
[10] Y. Gu and J. M. Yuan, Phys. Rev. A **36**, 3788 (1987).